Society of Medical Education & Research

2022, Volume 2, Issue 2, Page No: 49-63
ISSN: 3108-4826

Journal of Medical Sciences and Interdisciplinary Research

Precision Boron Neutron Capture Therapy for CA19-9–Expressing Cancers: A Tumor Marker–Guided Approach

Clara Isabel Moreno[1]*, Javier Miguel Ortega[1]

[1]Department of Management, Faculty of Economics, University of Zaragoza, Zaragoza, Spain.

***E-mail** ✉ c.moreno.unizar@gmail.com

Abstract

Boron neutron capture therapy (BNCT) offers a precision chemoradiation strategy by delivering boron compounds like p-borophenylalanine (BPA) into tumors via the L-type amino acid transporter 1 (LAT1). However, its effectiveness is constrained in tumors with low LAT1 expression. To expand the applicability of BNCT, we have developed a novel approach that leverages tumor-specific biomarkers, focusing on cancers that exhibit high levels of the validated glycan marker CA19-9. Using The Cancer Genome Atlas (TCGA) datasets, we explored the transcriptomic landscape to identify tumors with low LAT1 expression yet high levels of CA19-9. This analysis revealed that fucosyltransferase 3 (FUT3), the key enzyme driving CA19-9 synthesis, is upregulated in pancreatic, biliary, and ovarian cancers. Building on this insight, we designed a new boron agent, fucose-BSH, tailored to preferentially target CA19-9–positive tumors. Its chemical properties, pharmacokinetic behavior, tissue distribution, and therapeutic efficacy were systematically assessed in vitro and in xenograft models, with direct comparisons made to the established boron carrier, BPA. Fucose-BSH exhibited markedly higher boron accumulation in Cell lines positive for CA19-9, including HuCCT-1, AsPC-1, Panc 04.03, and HSKTC, and OVISE) than in the CA19-9–negative PANC-1 cell line. In HuCCT-1 xenograft models, boron levels in tumors reached 36.2 ppm, yielding a tumor-to-normal tissue ratio of 2.1 and surpassing the performance of BPA. Following neutron irradiation, BNCT mediated by fucose-BSH resulted in greater than 80% inhibition of tumor growth. Importantly, fucose-BSH maintained its therapeutic effectiveness in LAT1-deficient models, where BPA showed no efficacy, thereby verifying its LAT1-independent mechanism of targeting. This work introduces a precision BNCT strategy that exploits CA19-9 as a tumor-specific glycan for targeted boron delivery. The novel agent fucose-BSH demonstrates potential to extend BNCT applicability to LAT1-low cancers, including those of the pancreas, biliary tract, and ovary. These results offer a clinically relevant framework for tumor marker–guided chemoradiation and pave the way for translational implementation of BNCT. Moreover, this approach could facilitate the development of companion diagnostics and enable precision patient stratification in current and future BNCT clinical studies. Cancers characterized by high CA19-9 expression, including pancreatic, biliary, and ovarian malignancies, are linked to poor outcomes and limited responsiveness to existing treatments. In this study, we introduce a tumor marker–guided approach to boron neutron capture therapy (BNCT), exploiting the biology of CA19-9 glycans for selective tumor targeting using fucose-BSH, a novel boron agent. Through transcriptomic analyses and preclinical evaluation, fucose-BSH demonstrated effective LAT1-independent boron delivery, robust BNCT-induced cytotoxicity, and preferential accumulation in CA19-9–positive models. These results highlight a precision chemoradiation strategy that expands BNCT to previously untreatable tumors and provides a clinically actionable framework for patient selection and therapeutic development in CA19-9–expressing cancers.

Keywords: BNCT, Novel agent fucose-BSH, Neutron irradiation, Fucosyltransferase 3

Access this article online https://smerpub.com/

Received: 15 April 2022; **Accepted:** 27 July 2022

How to cite this article: Moreno CI, Ortega JM. Precision Boron Neutron Capture Therapy for CA19-9–Expressing Cancers: A Tumor Marker–Guided Approach. J Med Sci Interdiscip Res. 2022;2(2):69-63. https://doi.org/10.51847/DOVY9ncwra

Introduction

Boron neutron capture therapy (BNCT) was first proposed by Dr. Gordon Locher in 1936 as a treatment modality in which a boron-containing drug, specifically 10B, is administered to cancer patients while the targeted site is simultaneously exposed to neutron irradiation. When concentrated in tumor cells, the boron undergoes a

nuclear reaction with neutrons, producing a cell-killing effect [1, 2]. The alpha particles (He) and lithium nuclei generated by this reaction have a limited range of approximately 10 μm, enabling precise delivery of 10B-containing agents to cancer cells without significant damage to adjacent normal tissue [3]. Since BNCT operates at the cellular level, successful therapy critically depends on selective uptake of boron compounds by tumor cells. Notably, the first BNCT application for recurrent head and neck cancer received approval under Japanese public health insurance [4]. Current boron agents employed in BNCT include p-boronophenylalanine (BPA) and sodium borocaptate (BSH) [5]. One widely used preparation involves conjugating boron with the amino acid phenylalanine (BPA) [4]. Given that phenylalanine is a substrate for melanin synthesis, Hatanaka *et al*. conducted BPA-BNCT clinical trials against malignant melanoma, which demonstrated therapeutic efficacy [6, 7]. Subsequent studies revealed that BPA uptake is mediated not only by melanoma cells but also by L-type amino acid transporters (LAT1), which are overexpressed in a variety of malignancies, including head and neck, brain, and skin tumors [8]. Despite this, there remains an urgent need for alternative boron agents, as BNCT efficacy heavily relies on boron delivery to tumor cells [9]. While BSH has a long history of clinical research, its limited tumor selectivity and poor cellular uptake have restricted its recent use. This limitation prompted the idea of developing a precision BNCT strategy using BSH in combination with tumor markers, thereby targeting a mechanism distinct from BPA.

Tumor markers are biological indicators of the presence of malignancy [10]. Clinically, they can be measured in plasma or other body fluids and represent biochemicals associated with tumor activity [11]. These markers may be produced directly by tumor cells (tumor-derived) or by the host in response to tumor presence (tumor-related) [12]. Tumor markers encompass a wide range of molecules, including cell surface antigens, cytoplasmic proteins, enzymes, hormones, oncofetal antigens, receptors, oncogenes, and their products [13, 14]. One widely studied tumor marker is carbohydrate antigen 19-9 (CA19-9), also referred to as sialyl-Lewis A (sLea). CA19-9 is a cell surface glycoprotein complex, initially identified in 1979 in the colon cancer cell line SW1116 using a mouse monoclonal antibody (1116-NS-19–9) [15, 16]. By 1982, the antigen was found to correspond to a monosialoganglioside-derived glycolipid, providing a basis for pancreatic cancer diagnosis and therapy. Koprowski *et al.* further characterized CA19-9 in the blood of pancreatic cancer patients, establishing it as a pancreatic cancer-specific antigen [16]. During the 1980s, elevated CA19-9 levels were observed not only in pancreatic cancer but also in other gastrointestinal malignancies, including biliary, gastric, and colorectal cancers. CA19-9 measurements have been performed in serum, saliva, pancreatic cyst fluid, ascites, pleural fluid, and bronchoalveolar lavage (BAL) fluid [15]. Today, CA19-9 is utilized alongside imaging, hematological, pathological, and genetic diagnostics for comprehensive clinical assessment.

The biosynthesis of CA19-9 involves the uptake of fucose and glucose into cells as GDP-L-fucose, which is then processed in the Golgi apparatus via fucosyltransferase 3 (FUT3), generating the DUPAN-2 antigen. Elevated urinary fucose has also been investigated as an early biomarker for pancreatic cancer, alongside serum CA19-9 [17]. Beyond early detection, CA19-9 serves as a biomarker throughout the treatment course, informing decisions before, during, and after therapy [18]. For example, in localized pancreatic cancer, surgery may be deferred if neoadjuvant chemotherapy (NAC) is applied and CA19-9 levels remain elevated, as postoperative outcomes are often poor [19]. Post-treatment prognosis is similarly monitored through serial CA19-9 measurements [20]. Regular CA19-9 evaluation, combined with imaging, remains critical for recurrence surveillance. Beyond its role as a biomarker, CA19-9 also contributes to tumor progression. It can interact with the extracellular matrix, activate the EGFR signaling pathway, and cooperate with oncogenes such as KrasG12D to promote pancreatic tumor growth [21, 22]. Additionally, CA19-9 binds E-selectin on peritoneal endothelial and mesothelial cells, facilitating metastasis [23]. These properties have driven the development of CA19-9-targeted therapies, including therapeutic antibodies, imaging agents, and nuclear medicine applications, highlighting the clinical significance of CA19-9-expressing malignancies [24-27].

Building on this rationale, we propose a novel boron-containing drug based on BSH, chemically conjugated to the core structure of CA19-9. This CA19-9–targeted boron agent represents a new BNCT strategy for pancreatic, biliary, and related cancers with elevated CA19-9 expression. By promoting selective tumor accumulation of boron, this approach aims to broaden BNCT indications and ultimately enhance therapeutic

efficacy and clinical outcomes for patients with CA19-9–expressing tumors.

Materials and Methods

Ethics statement

All procedures involving animals adhered to ARRIVE 2.0 guidelines and were approved by the ethics committees of Kyoto University's Institute for Integrated Radiation and Nuclear Science (KURNS, 2023–38) and Okayama University (OKU-2020706, 2021515). Mice were kept in plastic cages manufactured by Clare Japan, positioned on AP Anicon racks (Seiken Corp.), and maintained under tightly controlled conditions: temperatures ranging from 20 to 25 °C, 40%–60% relative humidity, a minimum of 50 air changes per hour, and a 12-hour light/dark schedule with lights turning on at 8:00. Housing density met standard animal welfare guidelines. Eco Chip CL-4163 bedding (CLEA Japan) was provided, and the animals had unlimited access to sterile water and an MF diet (Oriental Yeast Co.). All cage components—including ventilated cages, lids, feeders, water bottles, and bedding—were sterilized by autoclaving. Animals were verified to be free of infectious murine agents. The use of human clinical specimens at Okayama University Hospital was approved by the Ethics Committee (OKU-1903–037), and written informed consent was obtained from all patients.

Processing and data source

Clinical and gene expression information for 13 different tumor types was accessed from The Cancer Genome Atlas (TCGA) portal (https://portal.gdc.cancer.gov/). The expression patterns of SLC7A5 and FUT3 were examined using the cBioPortal for Cancer Genomics. Data on tumor cell lines relevant to CA19-9 production were obtained from the Cancer Cell Line Encyclopedia (CCLE) (https://sites.broadinstitute.org/ccle/). To assess protein homology, sequences were queried against the non-redundant protein (nr) database using BLAST, applying a 90% query coverage filter. The evolutionary context of the FucP protein was explored via the EggNOG v5.0 database (http://eggnog5.embl.de/), also using a 90% query coverage threshold. Finally, survival analyses were conducted through Kaplan-Meier Plotter (https://kmplot.com/analysis/) to evaluate clinical outcomes.

Synthesis of the ^{10}BSH fucose triacetate conjugate (2):

The thiolated boron cluster Na_2 [$10B_{12}H_{11}SH$] (64 mg, 0.31 mmol) was combined with 2,3,4-tri-O-acetyl-6-deoxy-α-L-galactopyranosyl bromide (36 mg, 0.10 mmol) in acetonitrile (6.7 mL) along with triethylamine (0.4 mL, 3.0 mmol). The mixture was left to react at ambient temperature under an argon atmosphere for three days. After this period, the insoluble fraction was removed by filtration and rinsed lightly with water to afford the desired ^{10}B-labeled sugar–borane conjugate: 1,2,3,4,5,6,7,8,9,10,11-undecahydro-12-(1-thio-β-L-fucopyranose 2,3,4-triacetate-S)-[10B]dodecaborate (2). The product was obtained as a pale solid in 15% yield (7.4 mg, 15 μmol) with 99% ^{10}B content. Characterization of compound 2: ^{1}H NMR (600 MHz, D_2O): Complex multiplet between δ 1.01–1.62 (11 H), doublet at δ 1.16 (3 H, J = 6.6 Hz), three singlets at δ 1.99, 2.12, 2.21 (3 H each), quartet at δ 4.01 (1 H, J = 6.6 Hz), triplet at δ 4.95 (1 H, J = 9.9 Hz), double doublet at δ 5.16 (1 H, J = 9.9, 3.0 Hz), and doublet at δ 5.28 (1 H, J = 3.0 Hz),^{11}B NMR (192 MHz, D_2O): Signals observed at δ −20.4, −16.9, −14.8, −10.4, ^{13}C NMR (150 MHz, D_2O): δ 16.0, 20.6, 20.7, 21.3, 71.2, 72.0, 73.3, 73.4, 86.5, 173.3, 174.0, 174.3, FT-IR (KBr pellet): Peaks at 2483, 1734, 1418, 1075, 1002, 736 cm^{-1}, ESI-TOF MS (m/z): Calculated for $C_{12}H_{28}{}^{10}B_{12}NaO_7S$ $[M + Na]^-$ 459.3011; found 459.2998.

Cell culture and cell lines

Human cancer cell lines—including pancreatic cancer Pancreatic cancer cell lines (PANC-1, AsPC-1, Panc 04.03, PK-45 H), along with HuCCT-1 (cholangiocarcinoma), HSKTC (Krukenberg tumor), and OVISE (ovarian cancer), were acquired from RIKEN BRC, ATCC, or JCRB Cell Bank.and maintained following the recommended culture conditions provided by each repository.

X-ray exposure and colony formation

To investigate how different cancer cell lines respond to radiation, HSKTC, PK-45 H, PANC-1, OVISE, HuCCT-1, and Panc 04.03 were exposed to X-ray doses ranging from 0 to 6 Gy using an MX-80Labo irradiator. After irradiation, the cells were allowed to grow for 14 days, forming colonies that were later visualized with crystal violet staining. Colony size and number were quantified using ImageJ software [28].

Analysis of CA19-9–positive human cells via immunocytochemistry

The distribution of BSH within cells was explored using immunocytochemistry. Cells were treated with fucose-BSH for 2, 6, or 12 hours, then fixed and labeled with an anti-BSH monoclonal antibody (provided by Osaka Prefectural University, Prof. M. Kirihata) and Alexa Fluor 594. To provide structural context, nuclei were counterstained with Hoechst 33,258, and actin filaments with phalloidin 488. Images were captured with a Zeiss LSM780 confocal microscope.

Measuring boron uptake

Intracellular boron content was quantified via inductively coupled plasma mass spectrometry (ICP-MS; Agilent 7900, Agilent Technologies, Santa Clara, CA, USA) following a previously established method [29]. These measurements were performed at the Institute of Plant Resources and Science, Okayama University.

Blocking fucose-BSH uptake

To examine the inhibition of fucose-BSH uptake, cells were cultured in media containing L-fucose at concentrations of 0.1–10 mM. Viability was measured at 24 and 48 hours using absorbance at 450 nm, and boron levels were determined after 48 hours via ICP. In additional experiments, cells were treated with the GLUT1 inhibitor WZB117 (1–10 μM) 24 hours after fucose-BSH treatment, with boron uptake measured another 24 hours later [29].

Pharmacokinetics in tumor models

All animal experiments were approved by Okayama University (OKU-2020706, OKU-2021515). Female BALB/c-nude mice (6–8 weeks old, 16–20 g, Japan CLEA, Inc.) were subcutaneously injected with 2×10^6 HuCCT-1 cells. After one week, fucose-BSH (100 mg/kg) was administered intraperitoneally. Mice were sacrificed at intervals between 0.5 and 4 hours, and boron levels in tumors and other organs were measured using ICP as described previously [29].

Neutron irradiation in vivo and in vitro

For cell-based experiments, cultures from Okayama University were transported to KURNS and irradiated 24 hours later. HuCCT-1 and PANC-1 cells received pre-treatment with 150 μM fucose-Ac-BSH or BPA. Neutron irradiation was conducted at 1 MW in a mixed mode at the KUR-HWNIF facility (Kyoto University Heavy Water Neutron Irradiation Facility). After exposure, cells were cultured for two weeks, and colony formation was evaluated using ImageJ analysis and crystal violet staining (n = 4) [28].

For in vivo experiments, 4-week-old female BALB/c-nu/nu mice were subcutaneously injected with 2×10^6 HuCCT-1 cells. Two weeks later, the mice were transported to KURNS, anesthetized using a medetomidine/midazolam/butorphanol cocktail, and administered BPA or fucose-BSH (100 mg/kg). Tumor regions were selectively irradiated at 5 MW for 12 minutes with LiF shielding protecting surrounding tissues. Tumor growth and body weight were monitored over time. All procedures were conducted under approvals from Kyoto University (KURNS 2023–38) and Okayama University (OKU-2021515, OKU-2020706).

RNA sequencing and statistical methods

Pancreatic cancer samples from Okayama University Hospital were subjected to RNA sequencing. Raw reads were processed with Fastp to remove low-quality sequences and then pseudoaligned to the GRCh38 reference genome using Kallisto. Gene expression levels were normalized via the GeTMM method implemented in edgeR, and differentially expressed genes were identified using NOISeq, applying thresholds of probability >0.8 and absolute log2 fold change >1. All sequencing data are publicly available in GEO under GSE214899. For statistical analyses, t-tests, Mann–Whitney U tests, and one- or two-way ANOVA were conducted in GraphPad Prism 9, with significance defined as $p < 0.05$ and $q < 0.1$.

Results and Discussion

Analysis of CA19-9 biosynthesis in tumors with high versus normal levels

The CA19-9 antigen is generated in the Golgi apparatus through enzymatic modification of N-acetylglucosamine, involving B3GALT5 (galactosyltransferase), ST3GAL3 (sialyltransferase), and FUT3 (fucosyltransferase) **(Figure 1a).** The resulting structure consists of N-acetylglucosamine (blue), galactose (yellow), sialic acid (purple), and L-fucose (red), as illustrated in **Figure 1b.**

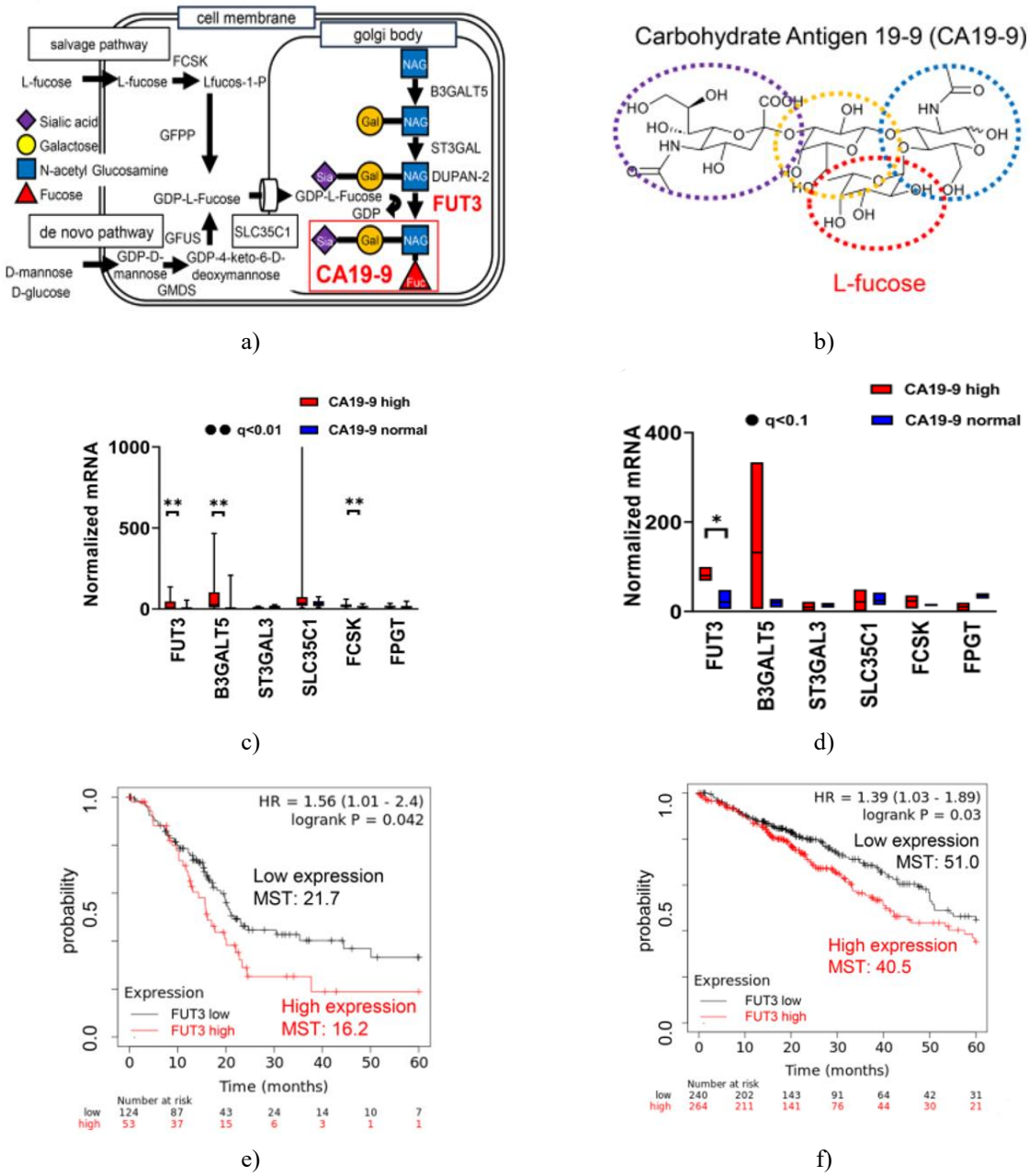

Figure 1. CA19-9 Biosynthesis and Clinical Significance of FUT3. (a) Overview of the enzymatic pathway responsible for producing carbohydrate antigen 19–9 (CA19-9). (b) Molecular structure of CA19-9, emphasizing L-fucose as a key monosaccharide component. (c) Transcriptomic comparison from the Cancer Cell Line Encyclopedia (CCLE) showing differential gene expression between cell lines with high versus normal CA19-9 levels ($q < 0.01$). (d) RNA sequencing of pancreatic tumors comparing cases with elevated CA19-9 and poor prognosis to cases with lower CA19-9 and better prognosis. (e) Survival analysis of PDAC patients based on FUT3 expression. (f) Survival analysis of lung adenocarcinoma patients stratified by FUT3 expression.

Analysis of CCLE data revealed that cell lines expressing high levels of CA19-9 also displayed markedly increased FUT3, B3GALT5, and FCSK transcripts (all $q = 0.003$) compared with CA19-9–normal lines **(Figure 1c).** In pancreatic tumor samples, FUT3 levels were elevated in the subset of patients with high CA19-9 and poorer outcomes, though the difference did not reach conventional significance ($q = 0.062$) **(Figure 1d).**

Kaplan–Meier analyses showed that PDAC patients with high FUT3 expression had a reduced median survival of 16.2 months, compared to 21.7 months for FUT3-low patients (HR = 1.56, p = 0.042) **(Figure 1e).** Similarly, lung adenocarcinoma patients with high FUT3 expression survived 40.5 months versus 51.0 months in the low-expression group (HR = 1.39, p = 0.03) **(Figure 1f).** These findings indicate that CA19-9 biosynthesis relies heavily on FUT3 and B3GALT5, and higher FUT3 expression is linked to poorer patient outcomes.

Analysis of LAT1 and FUT3 using TCGA data

To further explore molecular patterns, we examined the amino acid transporter LAT1 (SLC7A5) and FUT3 in TCGA datasets. Tumors with elevated CA19-9 showed lower LAT1 expression and higher FUT3 expression **(Figures 2a–2b).** Notably, an inverse relationship between LAT1 and FUT3 was observed in CA19-9–high PDAC (Spearman = −0.21, p = 9.75×10^{-3}) and esophageal adenocarcinoma (Spearman = −0.41, p = 9.13×10^{-9}) **(Figures 2c–2d).**

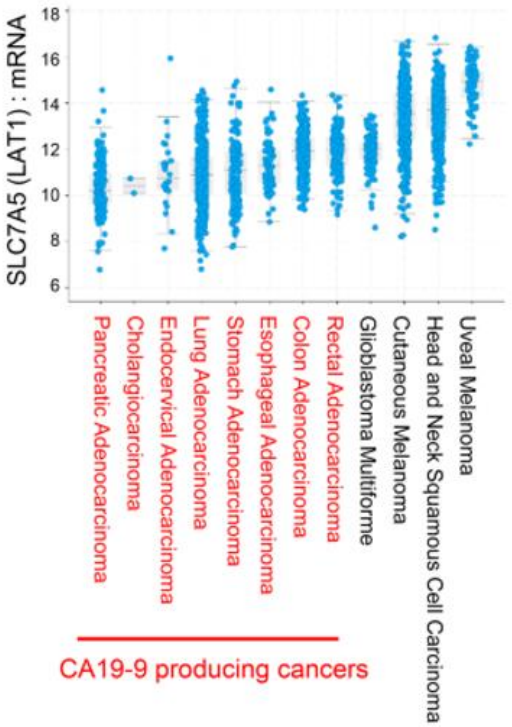

a)

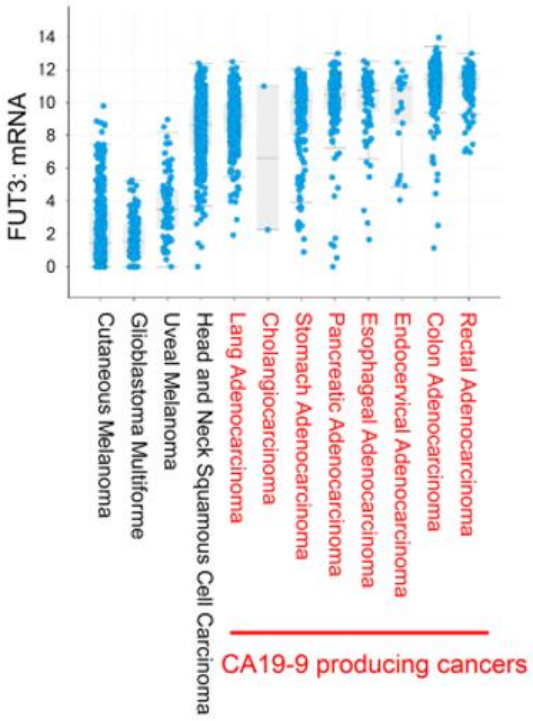

b)

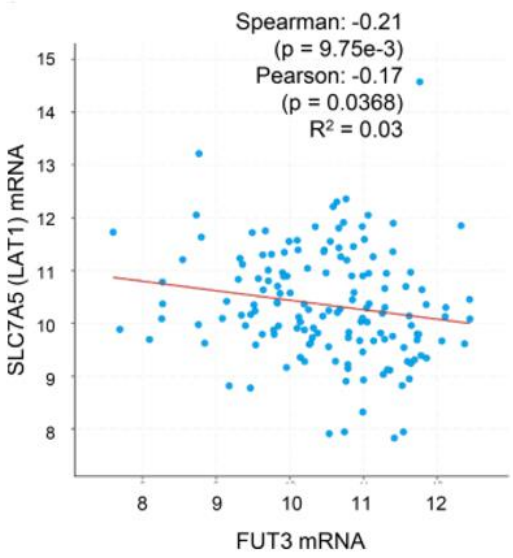

c)

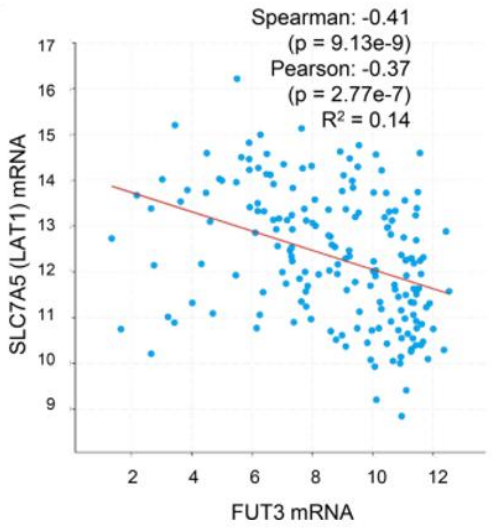

d)

Figure 2. LAT1 and FUT3 Patterns in CA19-9–Expressing Tumors. (a) Expression of LAT1 was profiled in CA19-9–high tumors using TCGA RNA-seq datasets. (b) In parallel, FUT3 expression was quantified in the same samples. (c) In PDAC, a pronounced negative correlation between LAT1 and FUT3 levels was observed. (d) A similar inverse relationship was detected in esophageal adenocarcinoma. Correlations were calculated using Spearman's rank method.

Analysis revealed that tumors producing elevated CA19-9 consistently exhibited reduced LAT1 levels alongside increased FUT3 expression. Interestingly, this inverse relationship appeared to be tumor type–specific, evident only in PDAC and esophageal adenocarcinoma. These findings suggest that the altered expression of LAT1 and FUT3 may constrain the utility of BPA-based therapeutic strategies in CA19-9–high cancers.

Synthesis of (fucose triacetate)-^{10}BSH conjugate 2 and incorporation in CA19-9–high tumors

The (fucose triacetate)-10BSH conjugate (2) was prepared by coupling 2,3,4-tri-O-acetyl-6-deoxy-α-L-galactopyranosyl bromide with ^{10}B-labeled mercaptoundecahydrododecaborate (10BSH, 1), yielding the desired product in 15% efficiency **(Figure 3a).** The structure of 2 was confirmed using ^{1}H NMR, ESI-TOF mass spectrometry **(Figure 3b)**, and IR spectroscopy**.**

In the ^{1}H NMR spectrum, resonances corresponding to the acetyl groups on fucose were observed at δ 1.99, 2.13, and 2.21 ppm, while the boron cage exhibited signals between δ 0.8–1.8 ppm. Mass spectrometry analysis detected a molecular ion at m/z 459.2998 ([M + Na]$^{-}$), consistent with the calculated mass of 459.3011 for $C_{12}H_{28}{}^{10}B_{12}NaO_7S$, confirming the successful formation of the conjugate.

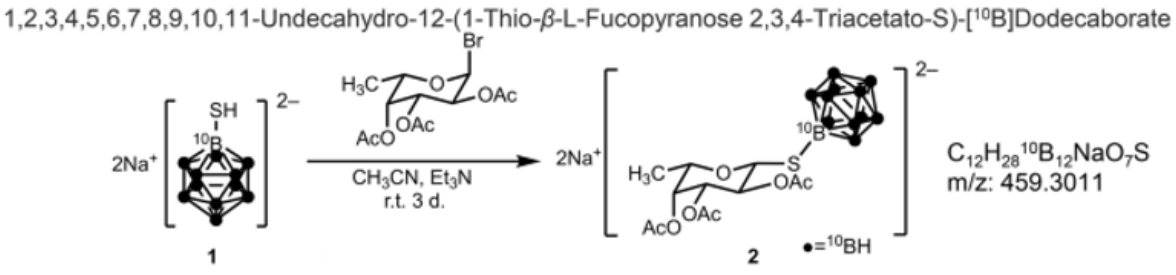

a)

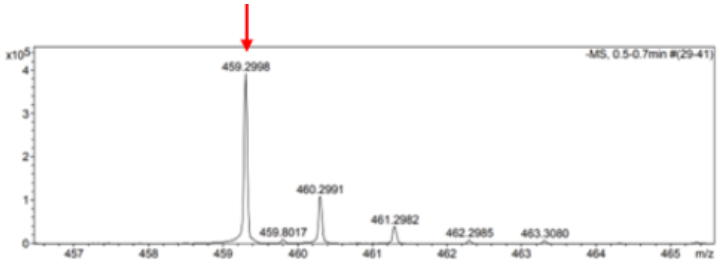

b)

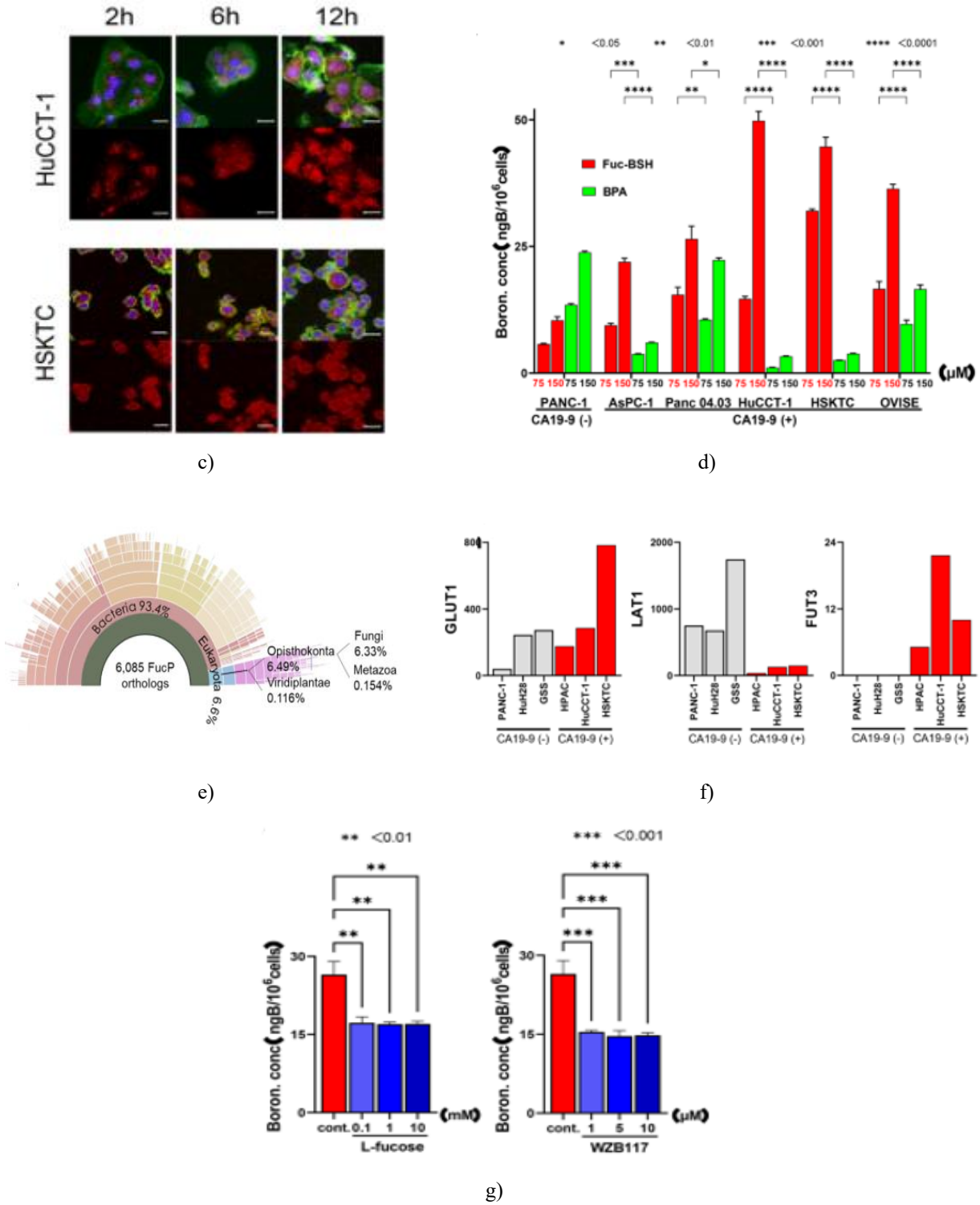

Figure 3. Design, Synthesis, and Cellular Delivery of a Fucose-Boron Conjugate. (a) Reaction pathway used to generate (fucose triacetate) [1] 10BSH (compound 2). (b) Mass spectrometric analysis confirming the molecular composition of compound 2. (c) Confocal imaging of CA19-9–positive cells treated with fucose-BSH at 2, 6, and 12 h. Red denotes BSH, green indicates phalloidin-stained cytoskeleton, and blue labels nuclei. Scale bar = 20 µm. (d) Quantification of intracellular boron after 24 h incubation with fucose-BSH or BPA, determined by ICP-MS (n = 4) in CA19-9–positive and –negative cells. (e) Phylogenetic mapping of the bacterial L-fucose

transporter (FucP) using EggNOG. (f) CCLE-based expression of GLUT1, LAT1, and FUT3 in CA19-9–positive versus CA19-9–negative cell lines. (g) Boron uptake in Panc 04.03(ng/10^6 cells ± sem) cells following pretreatment with L-fucose (left) or the GLUT1 inhibitor WZB117 (right), measured via ICP-MS (n = 4).

CA19-9–high HuCCT-1 and HSKTC cells were exposed to 150 µM fucose-BSH. Confocal microscopy revealed that the compound accumulated in both the cytoplasm and nucleus as early as 2 h and remained detectable at 6 and 12 h **(Figure 3c).** ICP-MS measurements after 24 h showed intracellular boron concentrations of 49.8 ± 1.9 (HuCCT-1), 44.7 ± 1.8 (HSKTC), 36.4 ± 0.9 (OVISE), 26.5 ± 2.5 (Panc 04.03), and 21.9 ± 0.7 ngB/10^6 cells (AsPC-1) **(Figure 3d).** Cells treated with BPA displayed significantly lower boron accumulation. In CA19-9–normal PANC-1, fucose-BSH produced 10.4 ± 0.7 ngB/10^6 cells, whereas BPA yielded 23.8 ± 0.2 ngB/10^6 cells. WST-8 cytotoxicity assays showed minimal variation across treatments**.**

Phylogenetic analysis revealed that the bacterial FucP transporter is widely conserved in prokaryotes but lacks homologs in humans, mice, frogs, and fish **(Figure 3e),** suggesting that mammalian fucose uptake relies on alternative transporters, including GLUT1. CCLE analysis indicated that CA19-9–positive cells generally express high GLUT1 and FUT3**,** but low LAT1: HPAC (GLUT1: 177.1, LAT1: 39.3, FUT3: 5.2), HuCCT-1 (GLUT1: 286.4, LAT1: 130.4, FUT3: 21.6), HSKTC (GLUT1: 783.6, LAT1: 151.3, FUT3: 10.0). In contrast, CA19-9–negative cells showed elevated LAT1 and lower FUT3 expression **(Figure 3f).**

Pretreating Panc 04.03 cells with L-fucose or GLUT1 inhibitor WZB117 reduced fucose-BSH uptake, with boron levels decreasing from 26.5 ± 2.5 (control) to 17.2 ± 1.2 (0.1 mM L-fucose), 17.0 ± 0.4 (1 mM), 17.0 ± 0.5 (10 mM), and 15.5 ± 0.3 (1 µM WZB117), 14.7 ± 1.0 (5 µM), 14.8 ± 0.5 ngB/10^6 cells (10 µM) (**Figure 3g)**. These results indicate that fucose-BSH entry is partially GLUT1-dependent**.**

In vitro assessment of neutron irradiation with fucose-BSH in CA19-9–high and –normal cells

Before initiating BNCT studies, we evaluated the radiation tolerance of six cancer cell lines by measuring colony formation after 2 Gy X-ray exposure. The surviving fractions (SF2) were as follows: HuCCT-1, 0.92; HSKTC, 1.00; Panc 04.03, 0.92; PK-45 H, 0.75; PANC-1, 0.81; OVISE, 0.66. confirming that all tested lines exhibit considerable resistance to ionizing radiation. For BNCT experiments, CA19-9–high HuCCT-1 and CA19-9–normal PANC-1 cells were exposed to fucose-BSH or BPA and subsequently irradiated with neutrons. Analysis of colony formation demonstrated that HuCCT-1 cells treated with fucose-BSH experienced a strong, dose-dependent reduction in survival, with significant inhibition observed at neutron fluences of 1.39 × 10^{12}, 2.59 × 10^{12}, and 4.14 × 10^{12} n/cm² ($p < 0.01$) **(Figure 4a).** Conversely, PANC-1 cells displayed no appreciable decrease in colony formation, even at a neutron fluence of 3.29 × 10^{12} n/cm² (Control: p = 0.95; BPA: p = 0.88) **(Figure 4b)**, indicating that the BNCT effect of fucose-BSH is selective for CA19-9–high cancer cells.

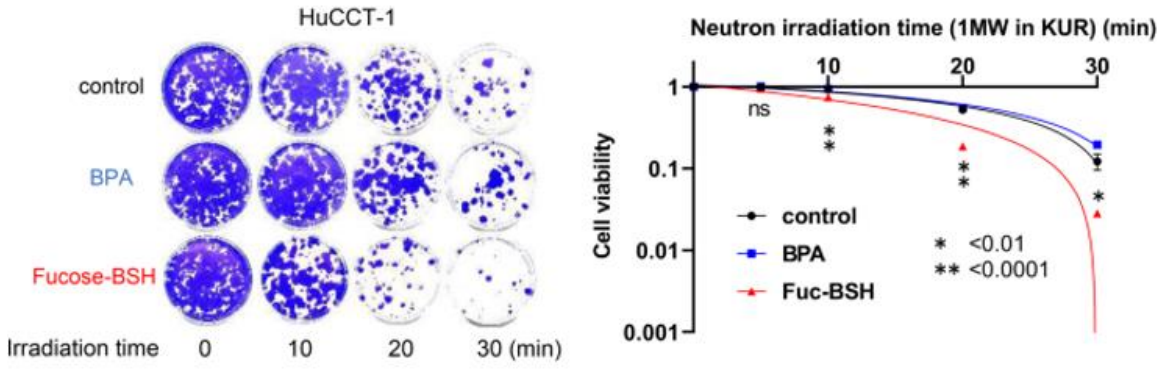

a)

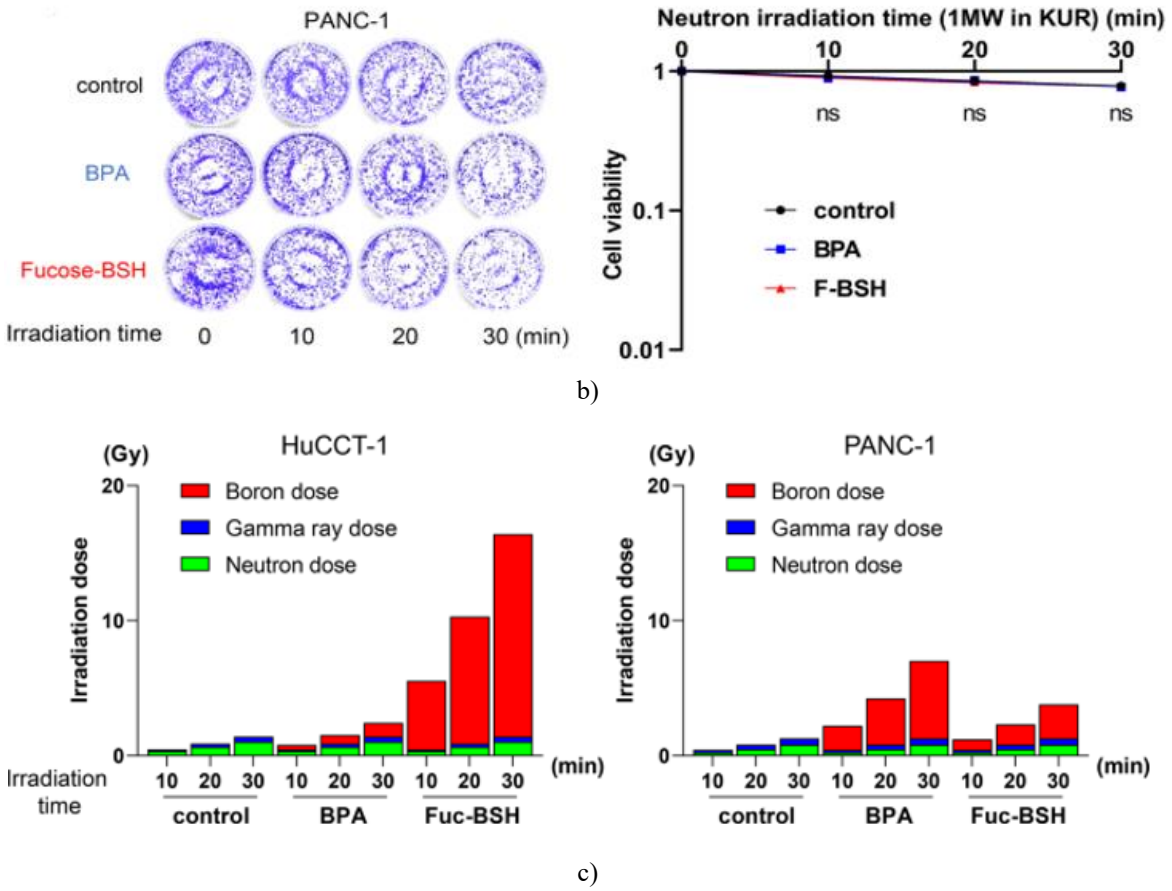

Figure 4. Selective cytotoxicity of fucose-BSH–mediated BNCT in CA19-9–positive and –negative cells. (a) Clonogenic assay results showing the survival of CA19-9–high HuCCT-1 cells after fucose-BSH treatment combined with neutron irradiation. (b) Survival analysis of CA19-9–low PANC-1 cells under the same experimental conditions. (c) Estimated absorbed BNCT doses (Gy) for each boron-containing compound. Data are expressed as mean ± SEM (n = 4). Significance: $p < 0.01$, $p < 0.001$. Neutron exposure duration (minutes) is indicated along the X-axis.

Dose calculations revealed that HuCCT-1 cells accumulated 5.6 Gy after 10 min, 10.3 Gy after 20 min, and 16.5 Gy after 30 min, while PANC-1 cells received substantially lower doses of 1.2 Gy, 2.3 Gy, and 3.8 Gy, respectively **(Figure 4c)**. These results indicate that fucose-BSH preferentially targets CA19-9–expressing cells, resulting in pronounced growth suppression**,** whereas CA19-9–negative cells remain largely unaffected.

Overall, fucose-BSH–mediated BNCT delivers greater effective boron doses to CA19-9–high cells, translating into enhanced cytotoxicity. In contrast, CA19-9–low PANC-1 cells, despite similar baseline radioresistance, exhibit minimal response. These findings underscore the potential of fucose-BSH as a selective boron delivery agent for CA19-9–positive malignancies**.**

Pharmacokinetics and BNCT outcomes of fucose-BSH in a CA19-9–high HuCCT-1 mouse model

The in vivo antitumor activity of fucose-BSH was assessed using BALB/c-nu/nu mice bearing HuCCT-1 xenografts. Mice received an intraperitoneal injection of fucose-BSH at 100 mg/kg, after which boron levels in tumors and multiple organs—including blood, brain, kidney, duodenum, muscle, skin, pancreas, and spleen—were quantified by ICP-MS at time points ranging from 0.5 to 4 hours.

Peak tumor accumulation of boron (36.2 ppm) occurred at 1 hour post-injection, while the skin and pancreas contained 34.6 ppm and 18.7 ppm**,** respectively. The tumor-to-normal tissue ratio for pancreas (T/N

(pancreas)) reached 2.1, indicating preferential accumulation in tumor tissue **(Figures 5a and 5b).**

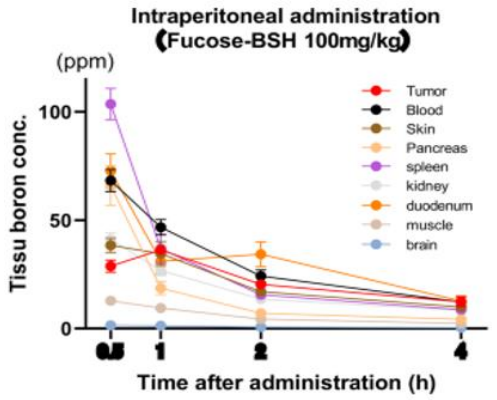

a)

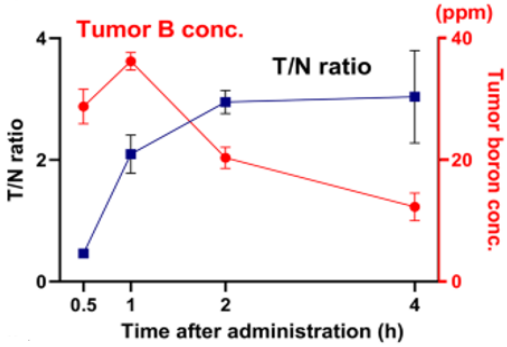

b)

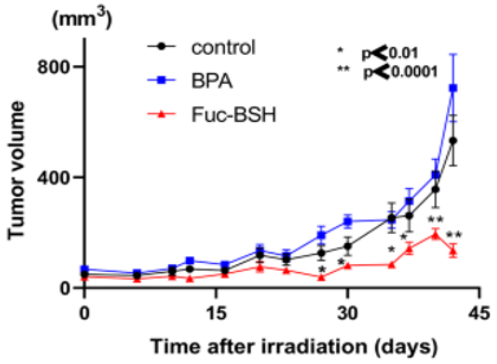

c)

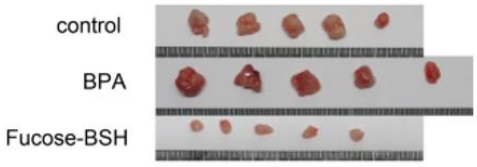

d)

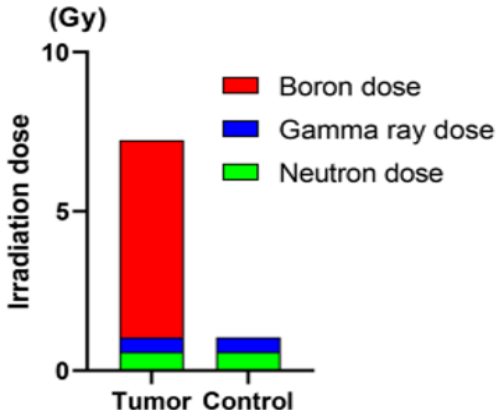

e)

Figure 5. Efficacy of Fucose-BSH–BNCT in HuCCT-1 Tumor-Bearing Mice. **(a)** Boron concentration (ppm ± SEM) measured in tumor tissues. **(b)** Ratio of tumor boron content to pancreatic tissue. **(c)** Tumor volumes (mm^3) monitored after neutron irradiation ($p < 0.01$, $p < 0.001$; n = 5 per group). **(d)** Representative photographs of subcutaneous tumors at 42 days post-BNCT. **(e)** Estimated tumor-absorbed dose (Gy) for fucose-BSH-BNCT versus control.

Mice transplanted with HuCCT-1 cells received fucose-BSH intraperitoneally (100 mg/kg). Neutron irradiation was carried out 1 hour after administration on day 14, with thermal neutron fluence ranging from 2.3–2.5 × 10^{12} n/cm^2 and epi-thermal fluence between 4.3–4.6 × 10^{12} n/cm^2.

Tracking tumor growth over time revealed that by day 42, the fucose-BSH-BNCT group had substantially reduced tumor size (135.6 ± 24.1 mm^3) compared with the untreated control (532.5 ± 91.2 mm^3) and BPA-BNCT (722.6 ± 121.3 mm^3) groups **(Figures 5c and 5d)**. The corresponding tumor-absorbed doses were 7.24 Gy for fucose-BSH-BNCT and 1.05 Gy for controls **(Figure 5e)**, indicating preferential boron delivery to tumor tissue.

These results demonstrate that fucose-BSH–mediated BNCT produces selective, potent antitumor effects in CA19-9–high HuCCT-1 xenografts, achieving higher tumor boron accumulation and superior growth inhibition compared with BPA-BNCT, supporting its potential as a safe and effective targeted therapy.

We have previously demonstrated that precision BNCT using glucose-BSH is effective against high-grade pancreatic cancer. In this study, we extended this

approach by integrating tumor marker information into drug design. By conjugating the boron-containing agent BSH to fucose, a core component of the tumor marker CA19-9, we synthesized fucose-BSH. This compound displayed selective uptake in CA19-9–high cancer cells and showed robust antitumor activity in both in vitro and in vivo neutron irradiation experiments. Furthermore, we observed that fucosyltransferase 3 (FUT3), essential for CA19-9 biosynthesis, exhibits an inverse correlation with LAT1, the transporter mediating BPA uptake.

While BPA-BNCT has proven effective in LAT1-high tumors, including melanoma, head and neck cancer, and malignant brain tumors [9], CA19-9 is generated when FUT3 transfers fucose onto its precursor DUPAN2. Notably, high FUT3 expression correlates with poor prognosis. In CA19-9–high tumors, FUT3 and LAT1 levels were inversely correlated **(Figures 6c and 6d),** suggesting that fucose-BSH targets a distinct population of cancer cells compared with BPA. Importantly, fucose-BSH demonstrated therapeutic efficacy in CA19-9–high malignancies, illustrating that BNCT can be refined to exploit tumor-specific markers. This strategy represents the first attempt to develop boron agents based on a component of CA19-9, enabling selective tumor accumulation beyond targeting highly expressed genes alone.

Elevated CA19-9 levels are recognized as a poor prognostic indicator in several cancers [30–33], motivating efforts to therapeutically lower CA19-9. Current approaches include the CA19-9–neutralizing antibody MVT-5873, evaluated in a phase I trial (NCT02672917) involving patients with stage III/IV pancreatic cancer, colorectal cancer, and unknown primary malignancies [34]. Notably, in pancreatic cancer patients receiving antibody plus chemotherapy, tumor suppression with subnormal CA19-9 levels was observed in three of six participants [25]. Additional strategies include radiolabeled antibodies, such as MVT-2163 for Immuno-PET imaging [26] and ^{177}Lu-labeled MAb 5B1 (MVT-1075) for therapeutic applications [27]. Furthermore, ^{225}Ac-labeled radioimmunotherapy targeting CA19-9 has been explored [21]. Despite these advances, therapies that directly target CA19-9–producing tumors remain extremely limited, emphasizing the novelty and potential of fucose-BSH-BNCT. Notably, combination therapy with CA19-9 antibodies could be pursued in the future.

In BNCT, the alpha particles and lithium nuclei generated from the ^{10}B-neutron reaction travel less than ~10 μm, necessitating precise delivery of boron to tumor cells while minimizing uptake in normal tissues. Clinical studies suggest that a tumor-to-normal tissue ratio (T/N) ≥ 2.0 is desirable [35], and a minimum tumor ^{10}B content of ~20 μg/g (~1 × 10^9 atoms/cell) is required for lethality [36]. Fucose-BSH achieved T/N ≥ 2.0 and tumor ^{10}B ≥ 20 ppm within 1 hour, meeting these practical requirements. Previous boron drug development strategies include polymeric drug delivery systems targeting surface markers, such as anti-EGFR immunoliposomes carrying BSH [37], and BPA-PVA complexes designed to retain BPA intracellularly for enhanced efficacy [38]. Fucose-functionalized nanoparticles have also been employed to deliver cisplatin to pancreatic cancer cells [39]. However, aside from our study, no reports have leveraged tumor markers and bioinformatics for boron drug discovery.

While CA19-9 served as the target in this work, therapies targeting tumor markers more broadly are expanding, particularly antibody-based approaches. For instance, anti-CA125 therapeutics have been evaluated for ovarian cancer, including nanotherapeutic implants conjugated to antibodies that improved survival in preclinical models [40, 41]. Similarly, CEA-targeted therapies, such as photoimmunotherapy and targeted alpha therapy (TAT) using ^{225}Ac or SN-38 conjugates, have demonstrated efficacy in colon cancer models [42–44]. These findings support the concept that fucose-BSH-BNCT selectively targets cell populations with high CA19-9 and, likely, elevated FUT3 expression. By extension, BNCT could be further optimized by exploiting other tumor-specific markers and gene expression patterns. To our knowledge, this is the first boron drug discovery effort focused on CA19-9 biosynthesis, illustrating the potential of precision BNCT guided by tumor biomarkers and patient-specific gene profiles.

Despite the promising results presented here, further investigations are warranted. Detailed analyses of boron distribution, radiation dose simulation, and pharmacokinetics are essential for accurately predicting BNCT's radiobiological effects [45]. Development of molecular imaging techniques, such as ^{18}F-FBPA PET, could complement these studies [46], and we are currently exploring PET-based evaluation of fucose-BSH pharmacokinetics using metal chelators (DOTA) [47]. Although BNCT is minimally invasive, potential effects on normal organs, especially during deep-tissue irradiation for CA19-9–high tumors, must be carefully considered. Open-abdominal neutron irradiation

approaches may be needed for future clinical translation [29].

Conclusion

In conclusion, fucose-BSH-based precision BNCT represents a novel therapeutic strategy for CA19-9–high malignancies. By exploiting FUT3-mediated fucose incorporation into CA19-9, we achieved selective tumor boron accumulation and demonstrated antitumor efficacy in vitro and in vivo. Understanding the mechanisms of fucose uptake and combining fucose-BSH-BNCT with conventional therapies could provide a multimodal treatment option for patients with CA19-9–high cancers and poor prognosis. Moving forward, validation in patient-derived xenograft (PDX) models and optimization of treatment timing may expand eligibility for surgical intervention and improve outcomes, particularly in pancreatic cancer. More broadly, our framework demonstrates that precision BNCT can be guided by tumor markers and gene expression profiles, offering a versatile platform for targeted cancer therapy beyond CA19-9.

Acknowledgments: None

Conflict of Interest: None

Financial Support: None

Ethics Statement: None

References

1. Locher GL. Biological effects and therapeutic possibilities of neutrons. Am J Roentgenol Radium Ther. 1936;36:1–13.
2. Nedunchezhian K, Aswath N, Thiruppathy M, Thirugnanamurthy S. Boron neutron capture therapy - a literature review. J Clin Diagn Res. 2016;10:ZE01–04.
3. Wongthai P, Hagiwara K, Miyoshi Y, Wiriyasermkul P, Wei L, Ohgaki R, Kato I, Hamase K, Nagamori S, Kanai Y. Boronophenylalanine, a boron delivery agent for boron neutron capture therapy, is transported by atb, LAT1 and LAT2. Cancer Sci. 2015;106:279–86.
4. Hirose K, Konno A, Hiratsuka J, Yoshimoto S, Kato T, Ono K, Otsuki N, Hatazawa J, Tanaka H, Takayama K, et al. Boron neutron capture therapy using cyclotron-based epithermal neutron source and borofalan ((10)B) for recurrent or locally advanced head and neck cancer (JHN002): an open-label phase ii trial. Radiother Oncol. 2021;155:182–87.
5. Miyatake S, Kawabata S, Kajimoto Y, Aoki A, Yokoyama K, Yamada M, Kuroiwa T, Tsuji M, Imahori Y, Kirihata M, et al. Modified boron neutron capture therapy for malignant gliomas performed using epithermal neutron and two boron compounds with different accumulation mechanisms: an efficacy study based on findings on neuroimages. J Neurosurg. 2005;103:1000–09.
6. Mishima Y, Honda C, Ichihashi M, Obara H, Hiratsuka J, Fukuda H, Karashima H, Kobayashi T, Kanda K, Yoshino K. Treatment of malignant melanoma by single thermal neutron capture therapy with melanoma-seeking 10B-compound. Lancet. 1989;2:388–89.
7. Snyder HR, Reedy AJ, Lennarz WJ. Synthesis of aromatic boronic acids. Aldehydo boronic acids and a boronic acid analog of Tyrosine1. J Am Chem Soc. 1958;80:835–38.
8. Kanai Y. Amino acid transporter LAT1 (SLC7A5) as a molecular target for cancer diagnosis and therapeutics. Pharmacol Ther. 2022;230.
9. Nakamura H. Historical development and current status of boron delivery agents for boron neutron capture therapy. Radioisotopes. 2015;64:47–58.
10. Bhatt AN, Mathur R, Farooque A, Verma A, Dwarakanath BS. Cancer biomarkers - current perspectives. Indian J Med Res. 2010;132:129–49.
11. Virji MA, Mercer DW, Herberman RB. Tumor markers in cancer diagnosis and prognosis. CA Cancer J Clin. 1988;38:104–26.
12. Nagpal M, Singh S, Singh P, Chauhan P, Zaidi MA. Tumor markers: a diagnostic tool. Natl J Maxillofac Surg. 2016;7:17–20.
13. Sharma S. Tumor markers in clinical practice: general principles and guidelines. Indian J Med Paediatr Oncol. 2009;30:1–8.
14. Zhou Y, Tao L, Qiu J, Xu J, Yang X, Zhang Y, Tian X, Guan X, Cen X, Zhao Y. Tumor biomarkers for diagnosis, prognosis and targeted therapy. Signal Transduct Target Ther. 2024;9:132.
15. Lee T, Teng TZJ, Shelat VG. Carbohydrate antigen 19–9 - tumor marker: past, present, and future. World J Gastrointest Surg. 2020;12.

16. Koprowski H, Steplewski Z, Mitchell K, Herlyn M, Herlyn D, Fuhrer P. Colorectal carcinoma antigens detected by hybridoma antibodies. Somatic Cell Genet. 1979;5:957–71.
17. Araki E, Kamiya K, Kawauchi A, Koike T, Takatsuka J, Takeuchi S, Namba M, Shida S, Ishiguro T, Tomoyoshi T, et al. Clinical assessment of urinary free L-fucose levels. Rinsho Byori. 1992;40:868–74.
18. Hartwig W, Strobel O, Hinz U, Fritz S, Hackert T, Roth C, Buchler MW, Werner J. CA19-9 in potentially resectable pancreatic cancer: perspective to adjust surgical and perioperative therapy. Ann Surg Oncol. 2013;20:2188–96.
19. Boone BA, Steve J, Krasinskas AM, Zureikat AH, Lembersky BC, Gibson MK, Stoller RG, Zeh HJ, Bahary N. Outcomes with FOLFIRINOX for borderline resectable and locally unresectable pancreatic cancer. J Surg Oncol. 2013;108:236–41.
20. Hata S, Sakamoto Y, Yamamoto Y, Nara S, Esaki M, Shimada K, Kosuge T. Prognostic impact of postoperative serum ca 19–9 levels in patients with resectable pancreatic cancer. Ann Surg Oncol. 2012;19:636–41.
21. Engle DD, Tiriac H, Rivera KD, Pommier A, Whalen S, Oni TE, Alagesan B, Lee EJ, Yao MA, Lucito MS, et al. The glycan CA19-9 promotes pancreatitis and pancreatic cancer in mice. Science. 2019;364:1156–62.
22. Wu Y, Liu F, Luo S, Yin X, He D, Liu J, Yue Z, Song J. Co-expression of key gene modules and pathways of human breast cancer cell lines. Biosci Rep. 2019;39.
23. Gebauer F, Wicklein D, Stübke K, Nehmann N, Schmidt A, Salamon J, Peldschus K, Nentwich MF, Adam G, Tolstonog G, et al. Selectin binding is essential for peritoneal carcinomatosis in a xenograft model of human pancreatic adenocarcinoma in pfp/rag2 mice. Gut. 2013;62:741–50.
24. Poty S, Carter LM, Mandleywala K, Membreno R, Abdel-Atti D, Ragupathi A, Scholz WW, Zeglis BM, Lewis JS. Leveraging bioorthogonal click chemistry to improve Ac-radioimmunotherapy of pancreatic ductal adenocarcinoma. Clin Cancer Res. 2019;25(3):868–880.
25. O'Reilly EM, Wang J-Z, Yu KH, Lowery MA, Varghese AM, Bendell JC, Borazanci EH, Estrella H, Fowler K, Hoskins M, et al. Abstract LB-B25: preliminary phase I data comparing HuMab-5B1 (MVT-5873), a monoclonal antibody targeting sLea, as a single agent and in combination with first line nab-paclitaxel and gemcitabine in patients with CA19-9 positive pancreatic cancer. Mol Cancer Ther. 2018;17:LB-B25–LB-B25.
26. Lohrmann C, O'Reilly EM, O'Donoghue JA, Pandit-Taskar N, Carrasquillo JA, Lyashchenko SK, Ruan S, Teng R, Scholz W, Maffuid PW, et al. Retooling a Blood-based Biomarker: phase I assessment of the high-affinity CA19-9 antibody HuMab-5B1 for immuno-PET imaging of pancreatic cancer. Clin Cancer Res. 2019;25:7014–23.
27. O'Reilly EA, Lohrmann C, O'Donoghue JA, Borazanci E, Estrella H, Teng R, Melink T, Dorr K, Kearns C, Peterson M, et al. Abstract CT140: phase I dose escalation study of 177Lu-HuMab-5B1 (MVT-1075) in combination with MVT-5873 as radioimmunotherapy (RIT) in subjects with relapsed/refractory pancreatic cancer or other CA19-9+ malignancies. Cancer Res. 2018;78:CT140–140.
28. Schneider CA, Rasband WS, Eliceiri KW. Nih image to ImageJ: 25 years of image analysis. Nat Methods. 2012;9:671–75.
29. Fujimoto T, Teraishi F, Kanehira N, Tajima T, Sakurai Y, Kondo N, Yamagami M, Kuwada A, Morihara A, Kitamatsu M, et al. BNCT pancreatic cancer treatment strategy with glucose-conjugated boron drug. Biomaterials. 2024;309:122605.
30. Hahn F, Muller L, Jungmann F, Mahringer-Kunz A, Tanyildizi Y, Duber C, Galle PR, Weinmann A, Kloeckner R. Survival prediction for patients with non-resectable intrahepatic cholangiocarcinoma undergoing chemotherapy: a retrospective analysis comparing the tumor marker ca 19–9 with cross-sectional imaging. J Cancer researchclin Oncol. 2020;146:1883–90.
31. Li Z, Zhuo Q, Li B, Liu M, Chen C, Shi Y, Xu W, Liu W, Ji S, Yu X, Xu X. Feasibility of laparoscopic versus open pancreatoduodenectomy following neoadjuvant chemotherapy for borderline resectable pancreatic cancer: a retrospective cohort study. World J Surg Oncol. 2024;22:1.
32. Wang F, Yuan X, Jia J, Bi X, Zhou Z, Zhou Q, Li X, Luo C, Deng M, Yi L, et al. Apatinib monotherapy for chemotherapy-refractory metastatic colorectal cancer: a multi-centre, single-arm, prospective study. Sci Rep. 2020;10:6058.
33. Zhu J, Jiang L, Wen H, Bi R, Wu X, Ju X. Prognostic value of serum CA19-9 and perioperative CA-125

levels in ovarian clear cell carcinoma. Int J Gynecol Cancer. 2018;28:1108–16.

34. Gupta S, McDonald JD, Ayabe R, Khan TM, Gamble LA, Sinha S, Hannah C, Blakely AM, Davis JL, Hernandez JM. Targeting ca 19–9 with a humanized monoclonal antibody at the time of surgery may decrease recurrence rates for patients undergoing resections for pancreatic cancer, cholangiocarcinoma and metastatic colorectal cancer. J Gastrointest Oncol. 2020;11:231–35.
35. Lan TL, Lin CF, Lee YY, Chang FC, Lin SC, Chou FI, Peir JJ, Pan PS, Chen JK, Lai LH, et al. Recurrent meningioma treated with boron neutron capture therapy: a feasibility study with dosimetric and clinical correlates. J Neurooncol. 2025;175:879–86.
36. Dymova MA, Taskaev SY, Richter VA, Kuligina EV. Boron neutron capture therapy: current status and future perspectives. Cancer Commun (lond). 2020;40:406–21.
37. Feng B, Tomizawa K, Michiue H, Miyatake S, Han XJ, Fujimura A, Seno M, Kirihata M, Matsui H. Delivery of sodium borocaptate to glioma cells using immunoliposome conjugated with anti-EGFR antibodies by ZZ-His. Biomaterials. 2009;30:1746–55.
38. Nomoto T, Inoue Y, Yao Y, Suzuki M, Kanamori K, Takemoto H, Matsui M, Tomoda K, Nishiyama N. Poly(vinyl alcohol) boosting therapeutic potential of p-boronophenylalanine in neutron capture therapy by modulating metabolism. Sci Adv. 2020;6:eaaz 1722.
39. Yoshida M, Takimoto R, Murase K, Sato Y, Hirakawa M, Tamura F, Sato T, Iyama S, Osuga T, Miyanishi K, et al. Targeting anticancer drug delivery to pancreatic cancer cells using a fucose-bound nanoparticle approach. PLoS One. 2012;7:e39545.
40. Mei L, Hou Q, Fang F, Wang H. The antibody-based CA125-targeted maintenance therapy for the epithelial ovarian cancer: a meta-analysis. Eur J Gynaecol Oncol. 2016;37:455–60.
41. Pantshwa JM, Rhoda K, Clift SJ, Pradeep P, Choonara YE, Kumar P, du Toit LC, Penny C, Pillay V. Chemotherapeutic efficacy of implantable antineoplastic-treatment protocols in an optimal mouse Model for human ovarian carcinoma cell targeting. Int J Mol Sci. 2018;19.
42. Shirasu N, Yamada H, Shibaguchi H, Kuroki M, Kuroki M. Potent and specific antitumor effect of CEA-targeted photoimmunotherapy. Int. J. Cancer. 2014;135:2697–710.
43. Minnix M, Kujawski M, Poku E, Yazaki PJ, Wong JY, Shively JE. Improved tumor responses with sequential targeted alpha-particles followed by interleukin 2 Immunocytokine therapies in treatment of CEA-Positive breast and colon tumors in cea transgenic mice. J Nucl Med. 2022;63:1859–64.
44. Nessler I, Rubahamya B, Kopp A, Hofsess S, Cardillo TM, Sathyanarayan N, Donnell J, Govindan SV, Thurber GM. Improving intracellular delivery of an antibody-drug conjugate targeting carcinoembryonic antigen increases efficacy at clinically relevant doses in vivo. Mol Cancer Ther. 2024;23:343–53.
45. Ono K, Tanaka H, Tamari Y, Watanabe T, Suzuki M, Masunaga SI. Proposal for determining absolute biological effectiveness of boron neutron capture therapy-the effect of 10B(n, alpha)7Li dose can be predicted from the nucleocytoplasmic ratio or the cell size. J Radiat Res. 2019;60:29–36.
46. Ishiwata K, Ido T, Kawamura M, Kubota K, Ichihashi M, Mishima Y. 4-Borono-2-[18F]fluoro-D, L-phenylalanine as a target compound for boron neutron capture therapy: tumor imaging potential with positron emission tomography. Int J RAD Appl Instrum B. 1991;18:745–51.
47. Iguchi Y, Michiue H, Kitamatsu M, Hayashi Y, Takenaka F, Nishiki T, Matsui H. Tumor-specific delivery of BSH-3R for boron neutron capture therapy and positron emission tomography imaging in a mouse brain tumor model. Biomaterials. 2015;56:10–17